ACS Energy LETTERS

http://pubs.acs.org/journal/aelccp

Direct Observation of Nucleation and Growth Behaviors of Lithium by *In Situ* Electron Microscopy

Chunyang Wang,[‖] Han Wang,[‖] Lei Tao, Xinyi Wang, Penghui Cao,* Feng Lin, and Huolin L. Xin*

Cite This: *ACS Energy Lett.* 2023, 8, 1929−1935

Read Online

ACCESS | Metrics & More | Article Recommendations | Supporting Information

ABSTRACT: **Lithium metal anodes are the "Holy Grail" of next-generation high-energy-density Li batteries, yet the nucleation and growth kinetics of Li metal at the nanoscale still remain a myth. Here, by combining *in situ* electron microscopy and atomistic simulations, we decipher the nanoscale nucleation and growth mechanisms of Li metal on carbon. We find that upon nucleation, Li atoms rapidly aggregate to form droplet-shaped nanoparticles that incline to coalesce through diffusion-mediated fusion. Statistical observation shows that the Li nucleation follows a mixed nucleation mode different from conventional instantaneous or progressive nucleation model. With increased particle size, the droplet-like Li particles transform into faceted crystals driven by surface energy minimization. Atomistic calculations reveal that the size-dependent Li diffusivity facilitates the coalescence and morphological evolution of the Li particles. This liquid-to-solid-like transformation during deposition is completely reversible upon stripping. This work, by unraveling the fundamental nano- and atomic-scale pathways dominating Li metal nucleation and growth behaviors, offers new insights into the deposition/stripping mechanism of Li metal.**

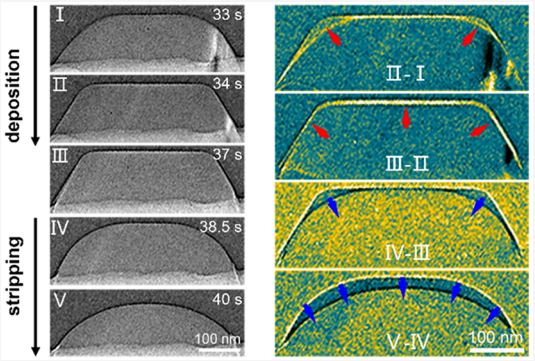

Lithium metal batteries have recently re-emerged with great research attention owing to the high theoretical specific capacity of 3860 mAh g^{-1} of Li metal.[1−3] However, the industrial application of Li metal batteries has been significantly plagued by poor cycling efficiency and severe safety concerns induced by uncontrollable Li dendrite growth.[4−8] To understand and suppress dendritic Li growth, considerable efforts have been made, including interface design and engineering,[9−12] fabrication of new host materials,[13,14] new electrolyte development,[15,16] and advanced tools for studying the growth of Li whiskers.[17−21] Because of its low density, high mechanical strength, high conductivity, and stable electrochemistry, carbon materials, e.g., 3D porous carbon,[22,23] interconnected carbon spheres,[24,25] carbon fibers, and membranes,[26,27] have been widely studied as host materials for Li anodes.[28] Besides, carbon surfaces modified by versatile lithiophilic functional groups such as oxygen-containing[27] or nitrogen-containing groups[25,26,29] have been developed to enable uniform Li deposition by preventing dendrite formation. For instance, Chen et al.[1] reported reversible deposition/stripping behavior of Li inside hollow tubules facilitated by Coble creep. However, so far, a fundamental understanding of the mechanisms underlying the nucleation, growth, and stripping kinetics of Li metal is yet to be established. Recently, by using cryogenic transmission electron microscopy, Wang et al.[30] reported that Li deposits with different structures, i.e., glassy Li and crystalline Li, are formed under varied deposition conditions. However, the *ex situ* nature of the experiments restrict us from visualizing the real-time microstructure evolution of Li metal during deposition/stripping with high spatial and high temporal resolution. It is still very challenging to capture the initial stage of Li deposition when Li metal begins to nucleate and subsequently grow into stable microstructures. Here, by combining *in situ* transmission electron microscopy and atomistic simulations, we resolve the nucleation−growth−stripping mechanism of Li metal on carbon surface in a working solid-state Li metal battery. We capture a liquid-like nucleation−coalescence growth pathway facilitated by fast surface diffusion for the first time. Moreover, a reversible droplet-like to faceting transition driven by surface

Received: January 24, 2023
Accepted: March 9, 2023
Published: March 27, 2023

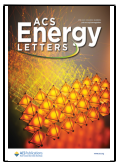

https://doi.org/10.1021/acsenergylett.3c00180
ACS Energy Lett. 2023, 8, 1929−1935

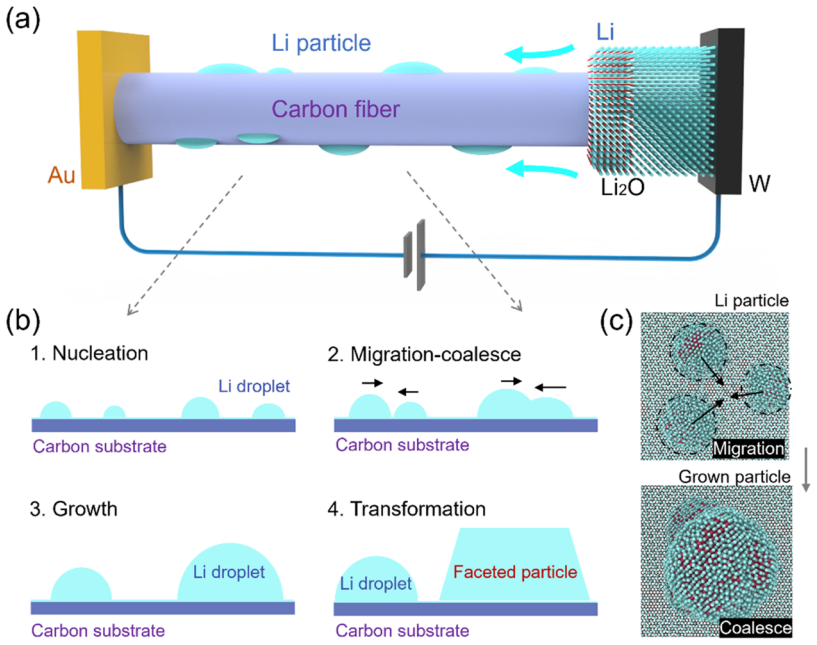

Figure 1. Nucleation−growth−stripping pathways of Li metal. (a) Schematic illustration of the scanning tunneling microscopy (STM)-TEM setup for *in situ* Li deposition and stripping. (b) Nucleation−coalescence-mediated Li growth and surface-energy-controlled faceting transition. (c) Li droplet migration and coalescence enabled rapid particle growth.

energy minimization is observed during Li deposition/stripping.

Figure 1a illustrates the experimental setup for the *in situ* deposition/stripping of Li metal on the carbon fiber functionalized with lithiophilic oxygen-containing groups to facilitate lithiation (see Experimental Methods in the Supporting Information). Based on time-resolved *operando* TEM, the growth−stripping mechanism of Li metal is uncovered and summarized in Figure 1b. We find that upon nucleation, Li atoms rapidly migrate and merge into droplet-shaped nanoparticles driven by diffusion-mediated fusion. During subsequent growth, the droplet-like Li particles transform into faceted crystals driven by surface energy reduction and local curvature modification. This surface-energy-controlled transformation is fully reversible upon stripping. In this work, a relatively low-dose imaging (see details in Experimental Methods) was adopted in our *in situ* observations to avoid beam damage (see Figures S1 and S2 and a discussion of the beam effect in Experimental Methods). Figure 2b shows the *in situ* observation of the nucleation and coalescence of Li nuclei upon deposition under a bias of −5 V (see a representative electron diffraction pattern of the Li nuclei in Figure S3). The coalescence of droplet-shaped Li nuclei (two or more) was found to occur through fusion on the carbon surface (indicated by yellow arrows). In the meantime, new nuclei (indicated by orange arrows) kept being generated (see schematic in Figure 2c). Figure 2d highlights the coalescence of two large Li particles with a size of ∼100 nm during *in situ* deposition. Aside from that, similar coalescence of Li nuclei with sizes of a few tens of nanometers was also captured (Figure 2e), indicating that coalescence took place both at the very beginning of nucleation and during subsequent growth of Li nuclei. Furthermore, the evolution of nuclei number and size during deposition was quantitatively investigated. Figure 2f shows the histogram of Li nuclei with different sizes on a single fiber and its evolution as a function of deposition time. It is seen that upon deposition, substantial nano nuclei instantaneously grew out from the surface and the number of nuclei kept increasing in a short time (from t = 0 to 0.2 s). Meanwhile, the rapid growth of Li nuclei resulted in scattered size distribution with increased average size, while the total number of nuclei stabilized shortly (t = 0.8 s) (see statistics from other carbon fibers in Figure S4). Different from the conventional instantaneous nucleation model[31] (the nucleation density first increases rapidly and then decreases) and the progressive nucleation model (the nucleation density increases progressively and then saturates), the Li nucleation behavior observed in this work follows somewhat a mixed nucleation mechanism, that is, instantaneous nucleation in the early stage followed by a saturation like in the scenario of progressive nucleation. The Li nucleation behavior is reproducible in cycles (see an example of Li deposition/stripping on a single carbon fiber for several cycles in Figure S5), and the Li deposition is also viable on multiple CNFs (see details in Figures S6−S8).

Furthermore, the growth and stripping behavior of Li metal was investigated in detail during discharge/charge cycling. Figure 3a presents time-resolved BF-TEM images (contrast inverted) showing the deposition and stripping of two Li particles with sizes less than 100 nm. With a bias applied, two Li particles grew out from the carbon surface with a droplet morphology in one second (t = 1 s, Figure 3a). Subsequently, with the bias reversed, the droplet-shaped Li particles were rapidly stripped off (t = 2s, Figure 3a). In another case, the growth and stripping of larger Li particles were also *in situ* tracked with prolonged deposition. Figure 3b shows the growth and stripping kinetics of a number of Li crystals with larger sizes (>100 nm). The Li crystals first adopted a droplet morphology (t = 2 s, Figure 3b) similar to that shown in Figure 3a. Later, with the increase of Li crystal size, facets (indicated by the arrows) started to form locally on Li crystal surfaces (t = 17.2 s, Figure 3b). With bias reversed, the Li crystals

https://doi.org/10.1021/acsenergylett.3c00180
ACS Energy Lett. 2023, 8, 1929−1935

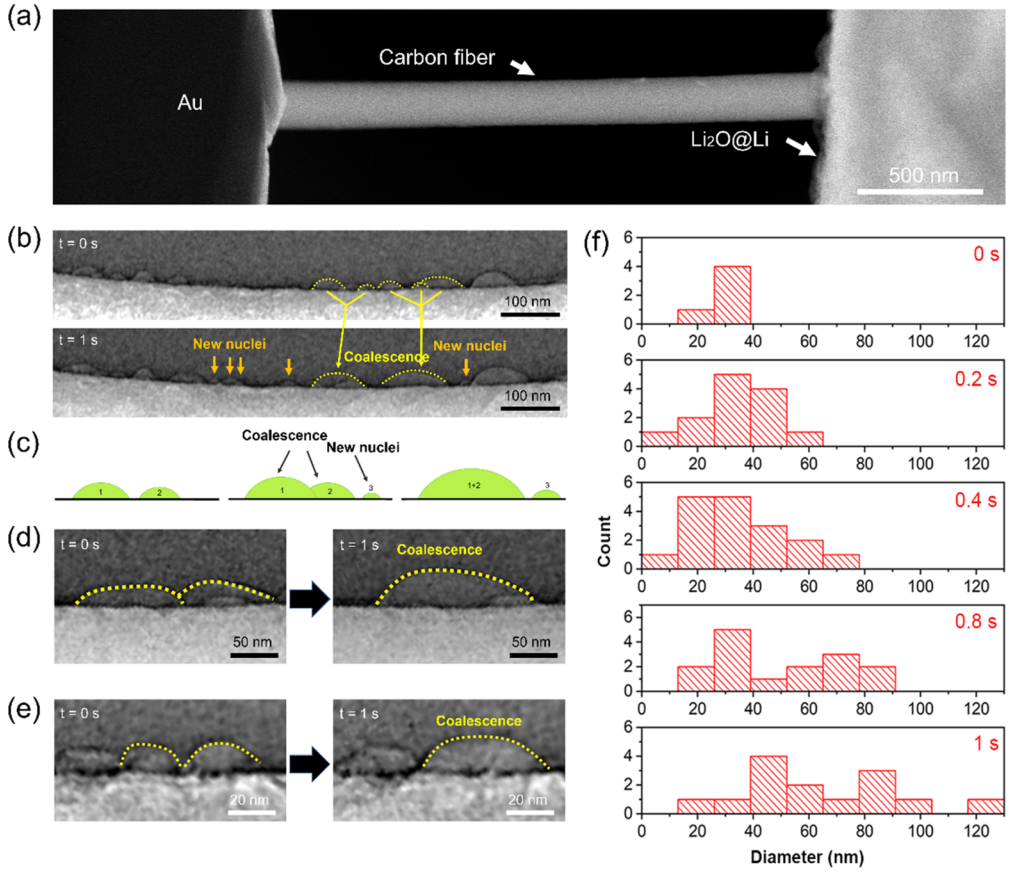

Figure 2. ***In situ*** **growth of Li through nucleation and coalescence of droplet-shaped Li nanoparticles. (a) Annular dark-field scanning transmission electron microscopy (ADF-STEM) image showing the** ***in situ*** **scanning tunnelling microscopy (STM)-TEM setup. (b) Time-resolved BF-TEM images (contrast inverted) show the** ***in situ*** **nucleation and coalescence of Li nuclei upon deposition. Coalesced and new nuclei are indicated by yellow and orange arrows, respectively. (c) Schematic illustration of the nucleation−coalescence growth pathway of Li metal during deposition. (d) Coalescence of two Li nuclei with the size of ∼100 nm during** ***in situ*** **deposition. (e) Coalescence of two Li nuclei with the size of ∼30 nm after nucleation. (f) Time-resolved size/amount evolution of Li nuclei as a function of time at the very beginning of Li deposition. A bias of −5 V was applied for the deposition (see unmarked images in Figure S9).**

immediately recovered to droplet morphology and rapidly stripped off (t = 20 s, Figure 3b). In contrast, for Li crystal with a size up to a few hundred nanometers, a droplet-like → faceting transition was observed. Figure 3c shows the time-resolved BF-TEM images (contrast inverted) of a large-sized Li crystal during deposition and stripping (see details in Movie S1). To highlight the morphological change of the Li crystal between different frames, image subtraction processing was performed between neighboring images. Figure 3d shows images of II−V in Figure 3c subtracted by I−IV, respectively. Aside from that, to quantitatively describe the evolution of the Li particle, the projected area of the Li metal and the contact angle between Li and carbon are plotted as a function of time in Figure 3e. We found that upon discharge, a Li crystal rapidly nucleated and grew out from the carbon surface at a very high rate (∼5000 nm^2/s). At the beginning (t = 33 s, Figure 3c), the Li crystal shows similar growth behavior as that of smaller Li particles (Figure 3a). As deposition continued, a complete droplet-like → faceting transition occurred immediately on the entire particle indicated by the formation of three sharp facets (t = 34 s, Figure 3c; see a detailed discussion of the crystallographic information on the facets in the Supporting Information, Figures S10 and S11, and Table S1). After the transition, the growth of Li crystal slowed down and further growth proceeded through the nearly uniform expansion of the facets (indicated by the red arrows in III−II, Figure 3d). Subsequently, with the bias reversed, the particle transited back to a droplet-like morphology starting from the intersection (the intersection region has larger curvature) of the facets (indicated by the blue arrows in IV−III, Figure 3d) and then extended to the entire particle (V−IV, Figure 3d). It is worth noting that before the particle transited to completely droplet-shaped, it went through an intermediate state whereby both the volume and contact angle only underwent a slight decrease (the cyan region in Figure 3e). Subsequently, the particle completely transited back to droplet-like morphology, and the contact angle and volume of the particle started to decrease significantly. Finally, the droplet-shaped Li particle was rapidly stripped off with a nearly constant contact angle of approximately 30° (Figure S12). A similar reversible transition was also observed during the *in situ* growth and stripping of Li on the Li_2O SEI of the anode (Figure S13), indicating that the droplet-like → faceting transition is likely an intrinsic property of Li metal itself. Interestingly, faceted Li single crystals[32] were also recently observed in practical batteries, suggesting that the droplet-like → faceting transition observed in this work could possibly apply to real battery systems.

To reveal the nucleation and growth mechanisms from the atomic- to nano-scale, we performed atomistic simulations of Li deposition (see Experimental Methods) using the molecular

https://doi.org/10.1021/acsenergylett.3c00180
ACS Energy Lett. 2023, 8, 1929−1935

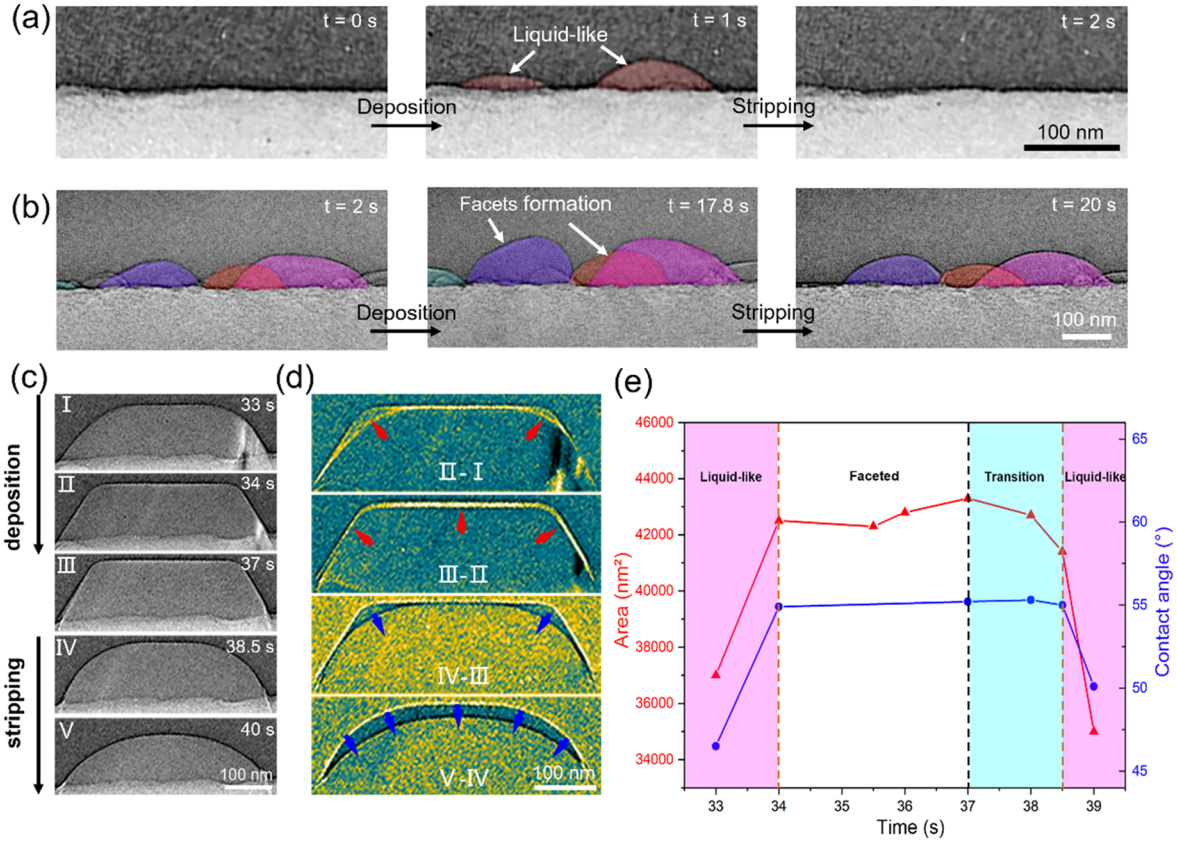

Figure 3. Reversible droplet-like → faceting transition of Li during *in situ* deposition and stripping. (a) Time-resolved BF-TEM images (contrast inverted) showing the growth and stripping of droplet-shaped Li particles with sizes below 100 nm. The two particles maintain droplet morphology throughout the deposition−stripping cycle. (b) Growth and stripping of relatively larger Li particles. The particles adopted droplet morphology in the beginning (t = 2 s), and then facets formed locally (indicated by arrows, t = 17.8 s). Upon stripping, the locally faceted particles transited back to droplet-shaped (t = 20 s). (c) Complete droplet-like → faceting transition of a large Li particle and its reversal upon stripping. (d) Images of II−V in panel c subtracted by I−IV highlighting the morphology change of Li particle during deposition and stripping process. Red and blue arrows indicate the growth and shrinkage direction, respectively. (e) Area and contact angle of the Li particle as a function of time during deposition and stripping. A bias of −5 V was applied for the Li deposition and 5 V for the stripping.

dynamics (MD) method coupled with Monte Carlo (MC). Figure 4a illustrates the four key stages underlying Li deposition, including nanocluster (amorphous) nucleation, cluster crystallization, cluster fusion, and particle growth (see details in Figure S14 and Movie S2). In the incipient stage of deposition, Li atoms quickly spread over the carbon surface and then condense into amorphous clusters. These nanosized clusters (A, B, and C shown in Figure 4a) grow with further deposition and soon transform into ordered body-centered cubic (BCC) particles (Figure 4b,c). The following stage, migration−fusion, occurs when the clusters' separation distance is reduced by cluster growth. Small clusters (B and C) captured by the large one (A) begin to migrate toward each other, followed by particle fusion. The small cluster B rearranges itself to align with the crystallographic orientation of the larger cluster A, while the cluster C retains its orientation, resulting in the formation of a bicrystal containing a grain boundary (Figure 4b). We hypothesize the formation of the bicrystal instead of a single crystal is attributed to the fast deposition rate and short simulation time limited by the MD method. Our hybrid MD and MC deposition simulation, which enables long time relaxation, confirms the hypothesis that the particle finally transforms into a single crystal (Figure S15). The annihilation of the grain boundary is driven by grain boundary migration, i.e., growth of one grain at the expense of the other in the bicrystal (see details in Movie S3). The processes of cluster fusion and subsequent recrystallization, occurring in a short time scale of 0.55 ns, suggest fast Li atom diffusion.

To understand atom diffusion and how it depends on particle size, we measured the mean squared displacement (MSD) and diffusivity of Li atoms in four different sized particles which are supported by carbon substrate, named as P1, P2, P3, and P4 (Figure S16). Their MSDs as a function of time are shown in Figure 4d. The diffusivity variation with particle size shown in Figure 4e demonstrates that the Li diffusivity increases rapidly as particle size decreases (see details in Table S2). For comparison and understanding the role of carbon substrate, the diffusivity of free-standing Li particles is calculated (Figure S17), which shows a drastically reduced value. The remarkable diffusivity of surface atoms in the Li particle, which is one order of magnitude higher than that of the overall particle, confirms the influential role of surface atoms and carbon substrate in facilitating particle migration and coalescence.

Theoretical analysis and atomic calculation were performed to understand the morphology transformation of the Li particles. We first derived the surface area relation of a

https://doi.org/10.1021/acsenergylett.3c00180
ACS Energy Lett. 2023, 8, 1929−1935

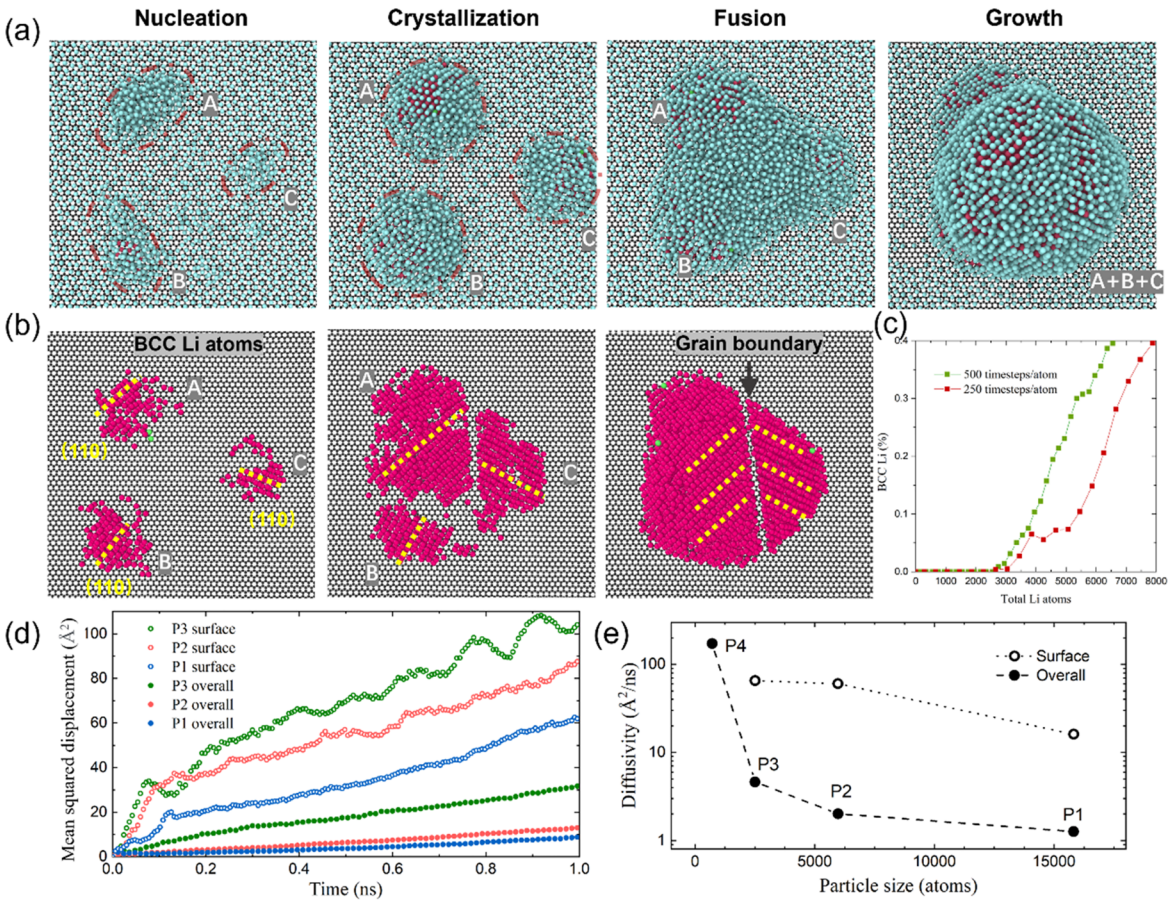

Figure 4. Atomistic simulations revealing the mechanisms underlying Li deposition and cluster-size-dependent diffusivity. (a) Sequential snapshots showing the four key stages, including nucleation, crystallization, fusion, and growth during Li deposition on carbon substrate. Body-centered cubic (BCC) and amorphous Li atoms are colored red and cyan, respectively. (b) Snapshots showing rearrangement of Li clusters during coalescence and the resultant bicrystal. Only BCC Li atoms are shown, and dashed lines indicate the (110) planes of BCC Li. (c) Fraction of BCC Li atoms as a function of total deposited Li. (d) Mean squared displacement (MSD) of Li against simulation time for particles P1, P2, and P3. The MSD associated with surface atoms is included for comparison. (e) Li diffusivity variation with particle size demonstrates increased diffusion with reducing particle size.

droplet-shaped particle and a faceted particle concerning the same volume. We assume the heights of the droplet-shaped domes and faceted particles (simplified as cubes) are half of the radius and the edge length, respectively (see schematics in Figure S18). So the surface areas of two particles, S_{droplet} and S_{faceted}, are given by

$$S_{\text{droplet}} = 2\pi rh = 2\pi r \times \frac{1}{2}r = \pi r^2 \tag{1}$$

$$S_{\text{faceted}} = 3a^2 \tag{2}$$

so the volumes of two particles, V_{droplet} and V_{faceted}, are

$$V_{\text{droplet}} = \frac{\pi h^2(3r - h)}{3} = \frac{\pi \frac{r^2}{4}\left(\frac{5}{2}r\right)}{3} = \frac{5\pi r^3}{24} \tag{3}$$

$$V_{\text{faceted}} = \frac{1}{2}a^3 \tag{4}$$

Rewriting S_{droplet} and S_{faceted} in terms of V_{droplet} and V_{faceted}, we see that

$$S_{\text{droplet}} = \pi r^2 = \pi\left(\frac{24V}{5\pi}\right)^{2/3} = C_1 V^{2/3} \tag{5}$$

$$S_{\text{faceted}} = 3(2V)^{2/3} = C_2 V^{2/3} \tag{6}$$

It is shown that given the same volume, the surface areas of the two droplets follow the same power-law relationship; thus, we speculate that the surface area difference itself will not drive the shape transition of Li particles. Next, we will consider the surface energy and local energy variations in the two shaped particles. Figure S19 shows the three typical particle sizes in this calculation, whose surface energy (per-area) and per-atom energy as a function of particle size are shown in Figure S20a and 20b, respectively. We can see that the droplet-like particle has a higher unit surface energy than the faceted particle. With the increase in particle size, the surface energy of both particles varies rapidly and then reaches a plateau. It means that if the particle shape morphology is governed by unit surface energy, the faceted shape is preferred as it has a lower value. When computing the total energy, due to the smaller surface area of the droplet-shaped particle, its total energy turns out to be smaller than that of the faceted particle (Figure S20e). The total energy comparison indicates that if the particle shape is dictated by total surface energy, the droplet shape is energetically preferred. In our experiments, we observe that the shape changes from droplet-like to faceted with increasing particle size. The observation implies that (1) for small

https://doi.org/10.1021/acsenergylett.3c00180
ACS Energy Lett. 2023, 8, 1929−1935

particles, the shape is influenced by minimizing the total surface energy and (2) for large particles, minimizing the local/unit surface energy governs the kinetics. This speculation is rational and can be interpreted by size-dependent diffusivity. We have shown that, with increasing particle size, the diffusion rate considerably reduces. This diffusion reduction limits the capability of diffusion-mediated shape evolution. As a result, as the particle size increases, the surface diffusion is merely able to modify the local curvatures to minimize the local surface energy, which enables the gradual shape transition from droplet-shaped to faceted particles.

The focus of this work is to understand the growth and stripping of nearly pure Li metal on carbon surfaces. Without obvious SEI formation, the Li nucleation and growth dynamics observed in our work more likely reflect the very incipient stage behavior of Li deposits when an SEI is not ready to or not effectively formed. However, we realize that the solid electrolyte interfaces (SEIs) widely existing in battery systems, especially those with liquid electrolytes, could make things more complicated. This is undoubtedly an important topic that deserves to be studied in the future. Broadly speaking, we conjecture that SEIs could influence the Li deposition and stripping pathways from two aspects. First, for the growth, if there is instantaneous SEI formation (the SEI formation rate varies from system to system) at the length scale of a few or a few tens of nanometers, which is the Li particles' length scales observed in this work, the growth behaviors or at least the kinetics could be changed because the SEI shell is very likely to hinder the coalescence of Li nuclei/particles. However, it is hard to tell to what degree the SEI can change the coalescence rates and kinetics. This is a very important topic that should be investigated in the future. Second, for the stripping, with the constraint (originating from the adhesion between Li and SEI) of an SEI shell on Li metal, the stripping kinetics of Li metal in SEI could be different from the case shown in this work, because the surfaces of Li crystals are not free anymore. In addition, even in the case when there is SEI formation, the variation of the length scale and components of SEI could also change the stripping modes. For example, we recently found that the ratio between the Li whisker diameter and SEI thickness could significantly change the mechanical stability of SEI as well as the Li stripping modes.[3] To sum up, the deposition and stripping of Li metal in real batteries is a complex phenomenon that could be influenced by many factors. To better understand Li transportation in practical batteries requires further development of more "practical" characterization techniques as well as the contribution from the whole community.

In conclusion, by combining *in situ* TEM and computational simulations, we capture the nucleation−coalescence growth behavior as well as a reversible droplet-like → faceting transition during *in situ* deposition/stripping of Li metal in a solid-state Li metal battery in TEM. Our findings provide a comprehensive understanding of the nucleation−growth−stripping kinetics of Li metal on carbon material. As the size-dependent growth/stripping behavior may also universally exist in other soft metals, e.g., sodium and potassium, the new findings in this work could be extended to other metal batteries.

■ ASSOCIATED CONTENT

Supporting Information

The Supporting Information is available free of charge at https://pubs.acs.org/doi/10.1021/acsenergylett.3c00180.

Experimental methods, TEM images of Li crystals under beam-blocked conditions, beam irradiation tests, electron diffraction of Li droplets, nucleation statistics, contact angle change as a function of time, reversible shape transition on anodes, MD simulation, surface energy calculation, and size-dependent diffusivity calculation (PDF)

Movie S1: Reversible droplet-like → faceting transition of a large-sized Li crystal (MP4)

Movie S2: MD simulation of the cluster crystallization, fusion, and particle growth (MP4)

Movie S2: Coalescence of Li crystals via grain boundary annihilation (MP4)

■ AUTHOR INFORMATION

Corresponding Authors

Penghui Cao − *Department Mechanical and Aerospace Engineering, University of California, Irvine, California 92697, United States;* orcid.org/0000-0001-9866-5075; Email: caoph@uci.edu

Huolin L. Xin − *Department of Physics and Astronomy, University of California, Irvine, California 92697, United States;* orcid.org/0000-0002-6521-868X; Email: huolin.xin@uci.edu

Authors

Chunyang Wang − *Department of Physics and Astronomy, University of California, Irvine, California 92697, United States;* orcid.org/0000-0001-8461-3952

Han Wang − *Department Mechanical and Aerospace Engineering, University of California, Irvine, California 92697, United States;* orcid.org/0000-0002-0179-6122

Lei Tao − *Department of Chemistry, Virginia Tech, Blacksburg, Virginia 24061, United States*

Xinyi Wang − *Department Mechanical and Aerospace Engineering, University of California, Irvine, California 92697, United States*

Feng Lin − *Department of Chemistry, Virginia Tech, Blacksburg, Virginia 24061, United States;* orcid.org/0000-0002-3729-3148

Complete contact information is available at: https://pubs.acs.org/10.1021/acsenergylett.3c00180

Author Contributions

[‖]C.W. and H.W. contributed equally to this work. H.L.X. conceived and directed the project. C.W. performed *in situ* TEM experiments and analysis. L.T. and F.L. synthesized the carbon fibers. P.C., H.W., and X.W. performed atomistic simulations. C.W., P.C., and H.L.X. wrote the Letter with help from all authors.

Notes

The authors declare no competing financial interest.

■ ACKNOWLEDGMENTS

This work is primarily supported by the National Science Foundation under award number DMR-2105328, and additional support received from HLX's startup funding. F.L. acknowledges the support from Virginia Tech Chemistry

Startup Funds. This research used the TEM facility of the Center for Functional Nanomaterials (CFN), which is a U.S. Department of Energy Office of Science User Facility, at Brookhaven National Laboratory under Contract No. DE-SC0012704. We thank Sooyeon Hwang and Kim Kisslinger for their help with the TEM experiments. We also thank Libing Yao and Huicong Yang for stimulating discussions.

REFERENCES

(1) Chen, Y.; Wang, Z.; Li, X.; Yao, X.; Wang, C.; Li, Y.; Xue, W.; Yu, D.; Kim, S. Y.; Yang, F.; et al. Li metal deposition and stripping in a solid-state battery via Coble creep. *Nature* **2020**, *578*, 251−255.

(2) Yan, K.; Lu, Z.; Lee, H.-W.; Xiong, F.; Hsu, P.-C.; Li, Y.; Zhao, J.; Chu, S.; Cui, Y. Selective deposition and stable encapsulation of lithium through heterogeneous seeded growth. *Nature Energy* **2016**, *1*, 16010.

(3) Wang, C.; Lin, R.; He, Y.; Zou, P.; Kisslinger, K.; He, Q.; Li, J.; Xin, H. L. Tension-Induced Cavitation in Li-Metal Stripping. *Advanced materials* **2023**, *35*, 2209091.

(4) Han, F.; Westover, A. S.; Yue, J.; Fan, X.; Wang, F.; Chi, M.; Leonard, D. N.; Dudney, N. J.; Wang, H.; Wang, C. High electronic conductivity as the origin of lithium dendrite formation within solid electrolytes. *Nature Energy* **2019**, *4*, 187−196.

(5) Li, L.; Basu, S.; Wang, Y.; Chen, Z.; Hundekar, P.; Wang, B.; Shi, J.; Shi, Y.; Narayanan, S.; Koratkar, N. Self-heating−induced healing of lithium dendrites. *Science* **2018**, *359*, 1513−1516.

(6) Gao, X.; Zhou, Y.-N.; Han, D.; Zhou, J.; Zhou, D.; Tang, W.; Goodenough, J. B. Thermodynamic Understanding of Li-Dendrite Formation. *Joule* **2020**, *4*, 1864−1879.

(7) Wu, B.; Wang, S.; Lochala, J.; Desrochers, D.; Liu, B.; Zhang, W.; Yang, J.; Xiao, J. The role of the solid electrolyte interphase layer in preventing Li dendrite growth in solid-state batteries. *Energy Environ. Sci.* **2018**, *11*, 1803−1810.

(8) Cheng, X. B.; Zhang, R.; Zhao, C. Z.; Zhang, Q. Toward Safe Lithium Metal Anode in Rechargeable Batteries: A Review. *Chem. Rev.* **2017**, *117*, 10403−10473.

(9) Sun, Y.; Liu, N.; Cui, Y. Promises and challenges of nanomaterials for lithium-based rechargeable batteries. *Nature Energy* **2016**, *1*, 16071.

(10) Kozen, A. C.; Lin, C.-F.; Pearse, A. J.; Schroeder, M. A.; Han, X.; Hu, L.; Lee, S.-B.; Rubloff, G. W.; Noked, M. Next-Generation Lithium Metal Anode Engineering via Atomic Layer Deposition. *ACS Nano* **2015**, *9*, 5884−5892.

(11) Zou, P.; Wang, C.; Qin, J.; Zhang, R.; Xin, H. L. A reactive wetting strategy improves lithium metal reversibility. *Energy Storage Materials* **2023**, DOI: 10.1016/j.ensm.2023.02.017.

(12) He, Y.; Zou, P.; Bak, S.-M.; Wang, C.; Zhang, R.; Yao, L.; Du, Y.; Hu, E.; Lin, R.; Xin, H. L. Dual Passivation of Cathode and Anode through Electrode−Electrolyte Interface Engineering Enables Long-Lifespan Li Metal−SPAN Batteries. *ACS Energy Letters* **2022**, *7*, 2866−2875.

(13) Yang, C. P.; Yin, Y. X.; Zhang, S. F.; Li, N. W.; Guo, Y. G. Accommodating lithium into 3D current collectors with a submicron skeleton towards long-life lithium metal anodes. *Nat. Commun.* **2015**, *6*, 8058.

(14) Lin, D.; Liu, Y.; Liang, Z.; Lee, H. W.; Sun, J.; Wang, H.; Yan, K.; Xie, J.; Cui, Y. Layered reduced graphene oxide with nanoscale interlayer gaps as a stable host for lithium metal anodes. *Nature Nanotechnol.* **2016**, *11*, 626−632.

(15) Cao, X.; Ren, X.; Zou, L.; Engelhard, M. H.; Huang, W.; Wang, H.; Matthews, B. E.; Lee, H.; Niu, C.; Arey, B. W.; et al. Monolithic solid−electrolyte interphases formed in fluorinated orthoformate-based electrolytes minimize Li depletion and pulverization. *Nature Energy* **2019**, *4*, 796−805.

(16) Pathak, R.; Chen, K.; Gurung, A.; Reza, K. M.; Bahrami, B.; Pokharel, J.; Baniya, A.; He, W.; Wu, F.; Zhou, Y.; et al. Fluorinated hybrid solid-electrolyte-interphase for dendrite-free lithium deposition. *Nat. Commun.* **2020**, *11*, 93.

(17) Kushima, A.; So, K. P.; Su, C.; Bai, P.; Kuriyama, N.; Maebashi, T.; Fujiwara, Y.; Bazant, M. Z.; Li, J. Liquid cell transmission electron microscopy observation of lithium metal growth and dissolution: Root growth, dead lithium and lithium flotsams. *Nano Energy* **2017**, *32*, 271−279.

(18) He, Y.; Ren, X.; Xu, Y.; Engelhard, M. H.; Li, X.; Xiao, J.; Liu, J.; Zhang, J. G.; Xu, W.; Wang, C. Origin of lithium whisker formation and growth under stress. *Nature Nanotechnol.* **2019**, *14*, 1042−1047.

(19) Zhang, L.; Yang, T.; Du, C.; Liu, Q.; Tang, Y.; Zhao, J.; Wang, B.; Chen, T.; Sun, Y.; Jia, P.; et al. Lithium whisker growth and stress generation in an in situ atomic force microscope−environmental transmission electron microscope set-up. *Nature Nanotechnol.* **2020**, *15*, 94−98.

(20) Sacci, R. L.; Dudney, N. J.; More, K. L.; Parent, L. R.; Arslan, I.; Browning, N. D.; Unocic, R. R. Direct visualization of initial SEI morphology and growth kinetics during lithium deposition by in situ electrochemical transmission electron microscopy. *Chem. Commun. (Camb)* **2014**, *50*, 2104−2107.

(21) Lin, R.; He, Y.; Wang, C.; Zou, P.; Hu, E.; Yang, X. Q.; Xu, K.; Xin, H. L. Characterization of the structure and chemistry of the solid-electrolyte interface by cryo-EM leads to high-performance solid-state Li-metal batteries. *Nature Nanotechnol.* **2022**, *17*, 768−776.

(22) Zhang, Y.; Wang, C.; Pastel, G.; Kuang, Y.; Xie, H.; Li, Y.; Liu, B.; Luo, W.; Chen, C.; Hu, L. 3D Wettable Framework for Dendrite-Free Alkali Metal Anodes. *Adv. Energy Mater.* **2018**, *8*, 1800635.

(23) Liu, S.; Wang, A.; Li, Q.; Wu, J.; Chiou, K.; Huang, J.; Luo, J. Crumpled Graphene Balls Stabilized Dendrite-free Lithium Metal Anodes. *Joule* **2018**, *2*, 184−193.

(24) Zheng, G.; Lee, S. W.; Liang, Z.; Lee, H. W.; Yan, K.; Yao, H.; Wang, H.; Li, W.; Chu, S.; Cui, Y. Interconnected hollow carbon nanospheres for stable lithium metal anodes. *Nature Nanotechnol.* **2014**, *9*, 618−623.

(25) Ye, W.; Pei, F.; Lan, X.; Cheng, Y.; Fang, X.; Zhang, Q.; Zheng, N.; Peng, D. L.; Wang, M. S. Stable Nano-Encapsulation of Lithium Through Seed-Free Selective Deposition for High-Performance Li Battery Anodes. *Adv. Energy Mater.* **2020**, *10*, 1902956.

(26) Niu, C.; Pan, H.; Xu, W.; Xiao, J.; Zhang, J. G.; Luo, L.; Wang, C.; Mei, D.; Meng, J.; Wang, X.; et al. Self-smoothing anode for achieving high-energy lithium metal batteries under realistic conditions. *Nature Nanotechnol.* **2019**, *14*, 594−601.

(27) Tao, L.; Xu, Z.; Kuai, C.; Zheng, X.; Wall, C. E.; Jiang, C.; Esker, A. R.; Zheng, Z.; Lin, F. Flexible lignin carbon membranes with surface ozonolysis to host lean lithium metal anodes for nickel-rich layered oxide batteries. *Energy Storage Materials* **2020**, *24*, 129−137.

(28) Ye, H.; Xin, S.; Yin, Y.-X.; Guo, Y.-G. Advanced Porous Carbon Materials for High-Efficient Lithium Metal Anodes. *Adv. Energy Mater.* **2017**, *7*, 1700530.

(29) Liu, L.; Yin, Y. X.; Li, J. Y.; Wang, S. H.; Guo, Y. G.; Wan, L. J. Uniform Lithium Nucleation/Growth Induced by Lightweight Nitrogen-Doped Graphitic Carbon Foams for High-Performance Lithium Metal Anodes. *Advanced materials* **2018**, *30*, 1706216.

(30) Wang, X.; Pawar, G.; Li, Y.; Ren, X.; Zhang, M.; Lu, B.; Banerjee, A.; Liu, P.; Dufek, E. J.; Zhang, J. G.; et al. Glassy Li metal anode for high-performance rechargeable Li batteries. *Nature materials* **2020**, *19*, 1339−1345.

(31) Pei, A.; Zheng, G.; Shi, F.; Li, Y.; Cui, Y. Nanoscale Nucleation and Growth of Electrodeposited Lithium Metal. *Nano Lett.* **2017**, *17* (2), 1132−1139.

(32) Wu, Z.; Wang, C.; Hui, Z.; Liu, H.; Wang, S.; Yu, S.; Xing, X.; Holoubek, J.; Miao, Q.; Xin, H. L.; Liu, P. Growing single-crystalline seeds on lithiophobic substrates to enable fast-charging lithium-metal batteries. *Nat. Energy* **2023**, DOI: 10.1038/s41560-023-01202-1.

https://doi.org/10.1021/acsenergylett.3c00180
ACS Energy Lett. 2023, 8, 1929−1935